High-precision determination of the electric and magnetic form factors of the proton

J. C. Bernauer,[1, *] P. Achenbach,[1] C. Ayerbe Gayoso,[1] R. Böhm,[1] D. Bosnar,[2] L. Debenjak,[3]
M. O. Distler,[1, †] L. Doria,[1] A. Esser,[1] H. Fonvieille,[4] J. M. Friedrich,[5] J. Friedrich,[1] M. Gómez Rodríguez
de la Paz,[1] M. Makek,[2] H. Merkel,[1] D. G. Middleton,[1] U. Müller,[1] L. Nungesser,[1] J. Pochodzalla,[1]
M. Potokar,[3] S. Sánchez Majos,[1] B. S. Schlimme,[1] S. Širca,[6, 3] Th. Walcher,[1] and M. Weinriefer[1]

(A1 Collaboration)

[1]*Institut für Kernphysik, Johannes Gutenberg-Universität Mainz, 55099 Mainz, Germany.*
[2]*Department of Physics, University of Zagreb, 10002 Zagreb, Croatia.*
[3]*Jožef Stefan Institute, Ljubljana, Slovenia.*
[4]*LPC-Clermont, Université Blaise Pascal, CNRS/IN2P3, F-63177 Aubière Cedex, France.*
[5]*Physik-Department, Technische Universität München, 85748 Garching, Germany*
[6]*Department of Physics, University of Ljubljana, Slovenia.*
(Dated: July 28, 2010)

New precise results of a measurement of the elastic electron-proton scattering cross section performed at the Mainz Microtron MAMI are presented. About 1400 cross sections were measured with negative four-momentum transfers squared up to $Q^2 = 1\,(\text{GeV}/c)^2$ with statistical errors below 0.2%. The electric and magnetic form factors of the proton were extracted by fits of a large variety of form factor models directly to the cross sections. The form factors show some features at the scale of the pion cloud. The charge and magnetic radii are determined to be $\langle r_E^2 \rangle^{\frac{1}{2}} = 0.879(5)_{\text{stat.}}(4)_{\text{syst.}}(2)_{\text{model}}(4)_{\text{group}}$ fm and $\langle r_M^2 \rangle^{\frac{1}{2}} = 0.777(13)_{\text{stat.}}(9)_{\text{syst.}}(5)_{\text{model}}(2)_{\text{group}}$ fm.

PACS numbers: 13.40.Gp, 14.20.Dh , 25.30.Bf

The proton is composed of relativistic light constituents, i.e. quarks and gluons, as manifest in "deeply inelastic" lepton scattering experiments. On the other hand, its global charge and magnetization distributions are contained in the form factors of elastic electron scattering. These provide a very instructive connection between models based on effective degrees of freedom and the QCD-based parton theory of the nucleon [1]. A particularly intriguing question is the existence of a direct signal for a pion cloud in the form factor hypothesized on the basis of pre-2003 data in Ref. [2]. Since Yukawa the virtual pion is considered as the mediator of the nucleon-nucleon force. Today it is viewed as an effective degree of freedom of the nucleon originating from the spontaneous breaking of chiral symmetry producing the Godstone bosons of QCD. An exciting question, addressed in this letter, is whether it could be seen directly.

A quantity particularly sensitive to the existence of a pion cloud is the proton charge radius. The determinations from electronic hydrogen Lamb shift measurements [3, 4] agree with those from e-p scattering if Coulomb and relativistic corrections are applied [5–7]. This work presents a novel determination of the electric and magnetic form factors and radii using a direct fit of form factor models to the electron scattering cross sections.

The Mainz accelerator MAMI provides a cw electron beam with energies up to 1600 MeV with very small halo and good energy definition. However, in this experiment only electron energies up to 855 MeV were used since the higher energies were not yet available at the time of the experiment. Taking advantage of the three high-resolution spectrometers of the A1 collaboration it was possible to measure the elastic electron-proton scattering cross section with a statistical precision of better than 0.2% and extract the form factors up to a negative four-momentum transfer squared of $Q^2 = 0.6\,(\text{GeV}/c)^2$.

About 1400 cross sections were measured at beam energies of 180, 315, 450, 585, 720, and 855 MeV covering Q^2 from 0.004 to $1\,(\text{GeV}/c)^2$. In order to achieve high accuracy the experiment aimed to maximize the redundancy of the data. For the angular scans the spectrometer angles were varied only in small steps so that the same scattering angle is measured up to 4 times with different regions of the spectrometer acceptance, and parts of the angular range were measured with two spectrometers. The broad range of beam currents from below 1 nA to more than 10 μA, a consequence of the large range of cross sections, required special attention to the determination of the luminosity. Therefore, the current was measured redundantly with a fluxgate magnetometer and with a pA-meter connected to a collimator just downstream the electron source. Furthermore, the relative luminosity was measured at all times with one of the three spectrometers at a fixed scattering angle.

In lowest order, the elastic electron-proton scattering cross section is described by the Rosenbluth formula

$$\left(\frac{\mathrm{d}\sigma}{\mathrm{d}\Omega}\right) = \left(\frac{\mathrm{d}\sigma}{\mathrm{d}\Omega}\right)_{\text{Mott}} \frac{\varepsilon G_E^2 + \tau G_M^2}{\varepsilon(1+\tau)}, \qquad (1)$$

where G_E and G_M are the electric and magnetic Sachs form factors, m_p is the proton mass, $\tau = Q^2/(4m_p^2 c^2)$ and $\varepsilon = \left(1 + 2\left(1+\tau\right)\tan^2(\theta/2)\right)^{-1}$ with the electron scatter-

ing angle θ. However, also electromagnetic processes of higher order contribute to the measured cross section, such as multiple photon exchange, vacuum polarization, vertex corrections, and the radiation of a real photon from the electron (Bethe-Heitler) or the proton (Born).

The code simulating the cross-section integration over the acceptance includes these processes following the description of ref. [8] which gives results compatible with ref. [9]. Our approach extends this by an explicit calculation of the Feynman graphs of the Bethe-Heitler and Born processes on the event level. The simulation uses the standard dipole parametrization

$$G_E = \frac{G_M}{\mu_p} = G_{\text{std. dip.}} = \left(1 + \frac{Q^2}{0.71(\text{GeV}/c)^2}\right)^{-2} \quad (2)$$

as a sufficient approximation for the true form factors (μ_p is the proton's magnetic moment divided by the nuclear magneton). The division of the measured number of elastically scattered electrons by luminosity and simulated acceptance-integrated (standard dipole) cross-section yields the measured normalized cross section; this procedure accounts for the radiative processes.

Furthermore, Coulomb corrections according to ref. [10] have been applied, but no correction for the exchange of two hard photons (TPE) in the scattering process since no unique prescription exists yet.

The energy of the elastically scattered electrons E_{out} is shifted by the recoil energy of the proton. The finite resolution of the spectrometers, the external energy-loss processes, and the internal bremsstrahlung widen the peak in the $\Delta E = E_{\text{out,calc.}} - E_{\text{out,meas.}}$ spectrum. The elastic events are selected by a cut around this peak.

The targets used were 2 and 5 cm long cells filled with liquid hydrogen with walls made of $10\,\mu\text{m}$ thick havar foil. The primary source of background is the elastic and quasielastic scattering off the nuclei in these walls. As verified with empty-cell measurements, inelastic peaks are either small or outside the cut region. The amplitude of its simulated shape was fitted to the measured ΔE spectrum together with the simulated hydrogen peak. As shown in Fig. 1 the simulated shapes describe the measured spectra very well. Therefore, after subtraction of the background from the raw spectra, the result is very insensitive to a variation of the cut around the elastic peak. In particular it shows the validity of the radiative corrections. The background contribution reaches up to 10% but is below 4% for most of the data.

For fixed Q^2 Eq. (1) can be rewritten as an equation of a straight line in ε in which G_E^2 and G_M^2 are fit parameters. This "Rosenbluth" method is model independent to first order in the photon propagator. However, one has to take the data at constant Q^2 for a sufficiently broad range of ε. For a given energy and angular range this limits severely the kinematical range covered. This restriction can be avoided by a direct least-squares fit of models
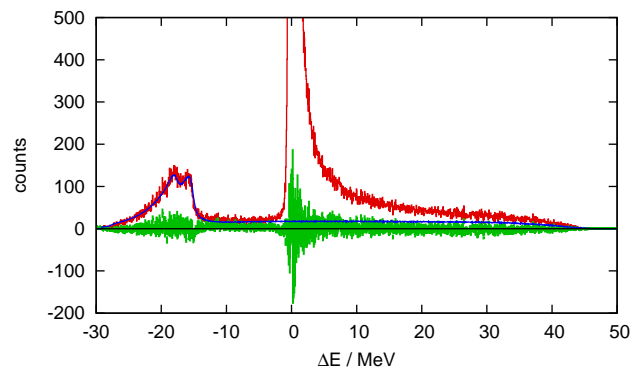

FIG. 1. Typical ΔE spectrum. Red histogram: measured spectra (height of elastic peak: 5500), blue line: simulated background, green shaded band: data minus simulated hydrogen peak and simulated background. The width of the band denotes the statistical uncertainty of the data. Data were measured at $E_0 = 450\,\text{MeV}$, $Q^2 = 0.045(\text{GeV}/c)^2$.

for G_E and G_M to the measured cross sections for all Q^2 and θ. Of course, it is mandatory to select a wide range of different models and test for any model dependence. In this work we have used single-dipole and sum-of-two-dipoles models, the phenomenological parametrization of ref. [2], several variations of polynomial, reciprocal of polynomial, and spline based models, and a variant of the extended Gari-Krümpelmann model [11]. A detailed study of the model dependence and the analysis method was performed using pseudo data generated according to a variety of previous parametrizations [2, 12, 13]. This study showed that all models with enough flexibility, i.e. polynomials, their reciprocals, and splines, are able to reproduce the input with an error smaller than the other systematic errors.

Since a determination of the absolute normalization of the measurement to better than 1% is not possible, the normalizations of the individual cross-section data sets are left as free parameters with the constraint $G_{E(M)}(Q^2 = 0) = 1(\mu_p)$. The fitted normalizations are well within the estimated uncertainty of 4% and have almost no dependency on the model. For the flexible models the spread between the largest and smallest normalization factor is below 0.3%.

The results of the direct fits are compatible with the results from a classic Rosenbluth separation where such a comparison is possible. However, we find that the Rosenbluth approach is more sensitive to systematic deviations and is therefore a less robust estimator of G_E^2 and G_M^2. However, the Rosenbluth separation allows us to check for deviations from a straight line caused by possible problems in the data or by higher-order processes like TPE. At the level of the uncertainty of the measurements no systematic deviations from straight lines were found.

As the direct fits of models are nonlinear, standard error estimation techniques for the fit are not guaranteed

to be exact. Therefore, the confidence bands were calculated with the Monte Carlo technique including the errors of the normalizations. We find that Monte Carlo and the linearization used in standard error propagation yield almost identical results for all but one model. The confidence bands presented here are the widely used pointwise bands, meaning that one expects the true curve to be with 68% probability within the band at any given single Q^2, but not necessarily at all Q^2 simultaneously. The Monte Carlo approach also allows one to construct simultaneous bands meaning that with 68% probability the true curve does not leave the band for the full range of Q^2. It is somewhat involved to treat this problem with standard analytical methods [14]. The simultaneous bands can be obtained from the pointwise bands shown here by scaling the latter by a factor of around 2.3 for the Q^2 range up to $0.6\,(\mathrm{GeV}/c)^2$.

The form factors extracted with the flexible models agree among each other to better than 0.25% in the Q^2 range up to 0.5 $(\mathrm{GeV}/c)^2$. They all fit the data equally well with $\chi^2/\mathrm{d.o.f.} \approx 1.14$ for d.o.f. ≈ 1400. However, including the less flexible models one obtains $1.16 \leqslant \chi^2/\mathrm{d.o.f.} \leqslant 1.29$ and the agreement is only better than 0.6%. In Fig. 2 the results of the spline model for G_E, G_M and their ratio are shown, together with previous measurements and fits. The error bars of the previous data shown for G_E and G_M are statistical only, normalization uncertainties are typically of the order of a few percent. Since TPE corrections are not applied to any of the data, the corresponding non-TPE-corrected fit of Ref. [13] is shown. In the plot of the ratio the fit to the TPE-corrected data of ref. [13] is also included.

The results for G_E exhibit a large negative slope relative to the standard dipole at $Q^2 \approx 0$ giving rise to the significantly larger charge radius. This slope levels out around $0.1\,(\mathrm{GeV}/c)^2$ and remains constant up to $0.55\,(\mathrm{GeV}/c)^2$ when the slope again becomes larger. In that region, however, only measurements at large scattering angles for only two beam energies contribute so that the fit becomes less reliable and more sensitive to systematic errors such as the neglect of TPE. For even higher Q^2 measurements have been taken only at one energy and a separation of G_E and G_M is not possible. In the close-up for G_E there is an indication of a bump around $0.15\,(\mathrm{GeV}/c)^2$, however, at the limit of significance.

The magnetic form factor G_M deviates from earlier measurements. This may be related to the normalization at $Q^2 \to 0$ ignoring the wiggle seen by this experiment. The maximum and the minimum of the wiggle structure depend, of course, on the parameter of the dipole form. Also, it is not clear whether the older experiments include the proton contribution to the radiative corrections.

The structure at small Q^2 seen in both form factors corresponds to the scale of the pion of about $Q^2 \approx m_\pi^2 \approx 0.02\,(\mathrm{GeV}/c)^2$ and may be indicative of the influence of the pion cloud [1].
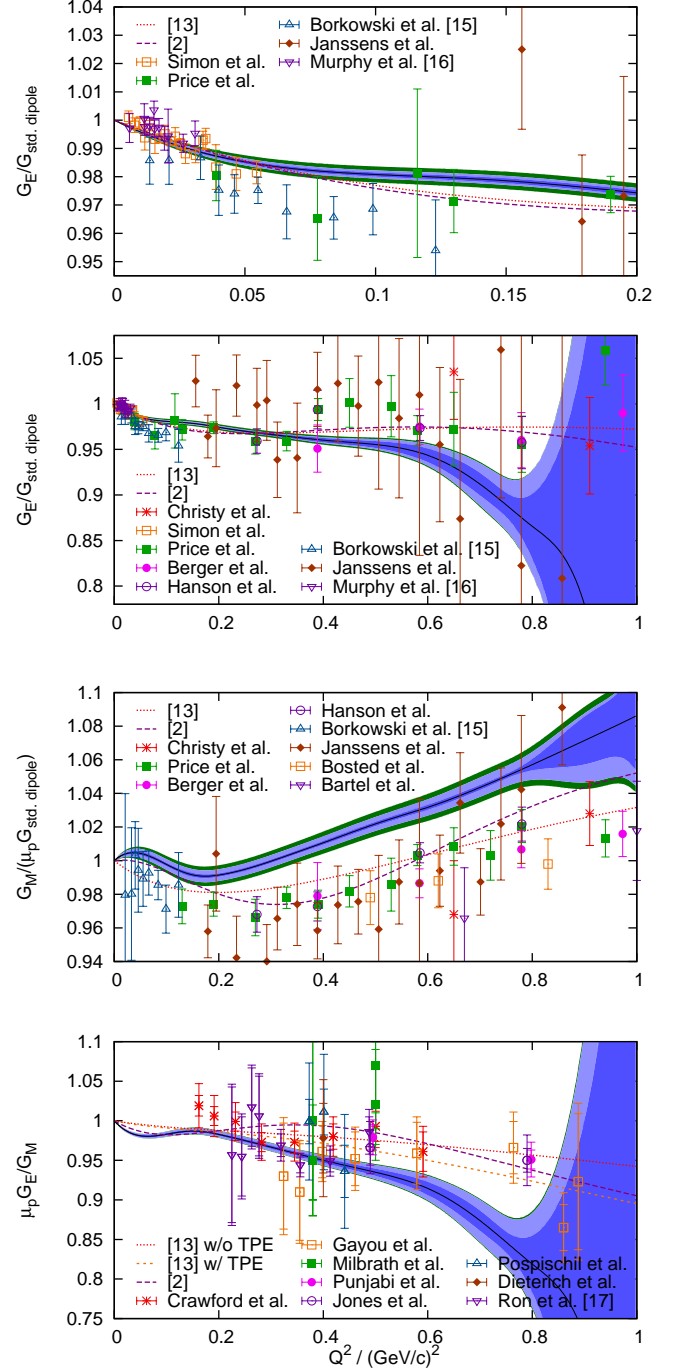

FIG. 2. The form factors G_E and G_M normalized to the standard dipole and G_E/G_M as a function of Q^2. Black line: best fit to the data, blue area: statistical 68% pointwise confidence band, light blue area: experimental systematic error, green outer band: variation of the Coulomb correction by $\pm 50\%$. The different data points depict previous measurements, for Refs. see [2, 13]; we added the data points of [15–17]. Dashed lines are previous fits to the old data in [2, 13].

While the deviation of G_M from previous measurements seems surprising at first glance, it reconciles the form factor ratios from experiments with unpolarized electrons, like this one, with those found with polarized electrons, especially with the high-precision measurements in ref. [17]. The previous G_E and G_M data are basically not compatible with the polarized measurements even when TPE corrections are applied. New results from Jefferson Laboratory [18, 19] with uncertainties of about 2% confirm this statement and are in excellent agreement with this experiment.

The charge and magnetic rms-radii are given by

$$\left\langle r_{E/M}^2 \right\rangle = -\frac{6\hbar^2}{G_{E/M}(0)} \left. \frac{\mathrm{d}G_{E/M}\left(Q^2\right)}{\mathrm{d}Q^2} \right|_{Q^2=0}. \quad (3)$$

In the study of the model dependency through simulated data only the flexible models reproduce the input radii reliably. In the fits to the measured data the models can be divided into two groups: Those based on splines with varying degree of the basis polynomial and number of support points and those composed of polynomials with varying orders. For the charge radius the weighted averages of the two groups differ by 0.008 fm.

For the spline group we obtain the values

$$\left\langle r_E^2 \right\rangle^{\frac{1}{2}} = 0.875(5)_{\text{stat.}}(4)_{\text{syst.}}(2)_{\text{model}} \, \text{fm},$$
$$\left\langle r_M^2 \right\rangle^{\frac{1}{2}} = 0.775(12)_{\text{stat.}}(9)_{\text{syst.}}(4)_{\text{model}} \, \text{fm}$$

and for the polynomial group

$$\left\langle r_E^2 \right\rangle^{\frac{1}{2}} = 0.883(5)_{\text{stat.}}(5)_{\text{syst.}}(3)_{\text{model}} \, \text{fm},$$
$$\left\langle r_M^2 \right\rangle^{\frac{1}{2}} = 0.778(^{+14}_{-15})_{\text{stat.}}(10)_{\text{syst.}}(6)_{\text{model}} \, \text{fm}.$$

Despite detailed studies the cause of the difference between the two model groups could not be found. Therefore, we give as the final result the average of the two values with an additional uncertainty of half of the difference:

$$\left\langle r_E^2 \right\rangle^{\frac{1}{2}} = 0.879(5)_{\text{stat.}}(4)_{\text{syst.}}(2)_{\text{model}}(4)_{\text{group}} \, \text{fm},$$
$$\left\langle r_M^2 \right\rangle^{\frac{1}{2}} = 0.777(13)_{\text{stat.}}(9)_{\text{syst.}}(5)_{\text{model}}(2)_{\text{group}} \, \text{fm}.$$

These radii have to be taken with the applied corrections in mind. While the Coulomb correction used is compatible with other studies [5, 6] a more sophisticated theoretical calculation may affect the results slightly.

The electric radius is in complete agreement with the CODATA06 [20] value of 0.8768(69) fm based mostly on atomic measurements. It is also in complete accord with the old Mainz result [21] when the Coulomb corrections [5, 6] are applied. However, the results from very recent Lamb shift measurements on muonic hydrogen [22] are 0.04 fm smaller, i.e. 5 standard deviations. This difference is unexplained yet. The calculation of the Lamb shift in muonic hydrogen requires the solution of a relativistic bound state problem (see Ref. [23] and references therein). The deviation may be due to the distorted wave functions, significantly more distorted than in electronic hydrogen, necessitating the consideration of multiphoton exchange.

The magnetic radius has a larger error than the charge radius since the experiment is less sensitive to G_M at low Q^2. Its value is smaller than results of previous fits, however, it is in good agreement with ref. [24], who found 0.778(29) fm from hyperfine splitting in hydrogen.

The consequences of the results presented here for our picture of the proton are discussed in ref. [1]. A full account of this work will be published [25, 26].

---

[*] bernauer@mit.edu; Present address: Laboratory for Nuclear Science, MIT, Cambridge, MA 02139, USA.
[†] distler@kph.uni-mainz.de
[1] M. Vanderhaeghen and Th. Walcher, (2010), to be published in Nuclear Physics News, arXiv:1008.4225 [hep-ph].
[2] J. Friedrich and Th. Walcher, Eur. Phys. J. A, **17**, 607 (2003), arXiv:hep-ph/0303054.
[3] K. Melnikov and T. van Ritbergen, Phys. Rev. Lett., **84**, 1673 (2000), arXiv:hep-ph/9911277.
[4] Th. Udem *et al.*, Phys. Rev. Lett., **79**, 2646 (1997).
[5] R. Rosenfelder, Phys. Lett. B, **479**, 381 (2000), arXiv:nucl-th/9912031.
[6] I. Sick, Phys. Lett. B, **576**, 62 (2003), arXiv:nucl-ex/0310008.
[7] P. G. Blunden and I. Sick, Phys. Rev. C, **72**, 057601 (2005), arXiv:nucl-th/0508037.
[8] M. Vanderhaeghen *et al.*, Phys. Rev. C, **62**, 025501 (2000), arXiv:hep-ph/0001100.
[9] L. C. Maximon and J. A. Tjon, Phys. Rev. C, **62**, 054320 (2000), arXiv:nucl-th/0002058.
[10] Y.-S. Tsai, Phys. Rev., **122**, 1898 (1961).
[11] E. L. Lomon, Phys. Rev. C, **64**, 035204 (2001), arXiv:nucl-th/0104039.
[12] J. Arrington, Phys. Rev. C, **69**, 022201 (2004), arXiv:nucl-ex/0309011.
[13] J. Arrington, W. Melnitchouk, and J. A. Tjon, Phys. Rev. C, **76**, 035205 (2007), arXiv:nucl-ex/0707.1861.
[14] J. C. Bernauer, M. O. Distler, J. Friedrich, and Th. Walcher, (2010), to be published.
[15] F. Borkowski *et al.*, Nucl. Phys. B, **93**, 461 (1975).
[16] J. J. Murphy, Y. M. Shin, and D. M. Skopik, Phys. Rev. C, **9**, 2125 (1974).
[17] G. Ron *et al.*, Phys. Rev. Lett., **99**, 202002 (2007), arXiv:nucl-ex/0706.0128.
[18] D. W. Higinbotham, AIP Conference Proceedings, **1257**, 637 (2010).
[19] X. Zhan and D. W. Higinbotham, (2010), private communication and to be published.

[20] P. J. Mohr, B. N. Taylor, and D. B. Newell, Rev. Mod. Phys., **80**, 633 (2008), arXiv:physics.atom-ph/0801.0028.

[21] G. G. Simon *et al.*, Nucl. Phys. A, **333**, 381 (1980).

[22] R. Pohl *et al.*, Nature, **466**, 213 (2010).

[23] E. Borie, Phys. Rev. A, **71**, 032508 (2005), arXiv:physics/0410051.

[24] A.V. Volotka *et al.*, Eur. Phys. J. D, **33**, 23 (2005).

[25] J. C. Bernauer, Ph.D. thesis, Johannes Gutenberg-Universität Mainz (2010).

[26] J. C. Bernauer *et al.*, (2010), to be published.